JGR Space Physics

RESEARCH ARTICLE
10.1029/2018JA026201

Are EEP Events Important for the Tertiary Ozone Maximum?

Annet Eva Zawedde[1], Hilde Nesse Tyssøy[1], Johan Stadsnes[1], and Marit Irene Sandanger[1]

[1]Birkeland Centre for Space Science, Department of Physics and Technology, University of Bergen, Bergen, Norway

Key Points:
- MLS provides a unique opportunity to study the direct impact of energetic particle precipitation on mesospheric hydroxyl (OH) and ozone (O_3)
- There is limited overlap between the auroral zone and the tertiary O_3 maximum at twilight conditions
- The importance of energetic electron precipitation on the tertiary O_3 maximum is strongly governed by the background atmosphere

Correspondence to:
A. E. Zawedde,
Annet.E.Zawedde@uib.no

Citation:
Zawedde, A. E., Nesse Tyssøy, H., Stadsnes, J., & Sandanger, M. I. (2019). Are EEP events important for the tertiary ozone maximum? *Journal of Geophysical Research: Space Physics*, *124*, 5976–5994. https://doi.org/10.1029/2018JA026201

Received 15 OCT 2018
Accepted 26 MAY 2019
Accepted article online 5 JUN 2019
Published online 12 JUL 2019

©2019. The Authors.
This is an open access article under the terms of the Creative Commons Attribution-NonCommercial-NoDerivs License, which permits use and distribution in any medium, provided the original work is properly cited, the use is non-commercial and no modifications or adaptations are made.

Abstract Energetic particle precipitation (EPP) increases the production of odd hydrogen (HO_X) species in the mesosphere, which catalytically destroy ozone (O_3) in sunlight. Hence, the EPP-HO_X impact on the tertiary O_3 maximum (TOM) depends on a complex geometry of a geographic-oriented TOM, geomagnetic-oriented auroral zone, producing short-lived HO_X species, and a destruction process depending on the solar zenith angle (SZA). Particle observations from the Medium Energy Proton and Electron Detectors telescopes aboard the Polar Orbiting Environmental Satellites, and hydroxyl (OH) and O_3 mixing ratios from Aura microwave limb sounder (MLS) are used to investigate the potential limitations of using the MLS observations to study EPP-OH impact on the TOM in the Northern Hemisphere. Our results show limited overlap between the auroral zone and the TOM at twilight conditions. A composite analysis indicates O_3 mixing ratio decrease over the auroral zone lagged by ~1 day compared to the maximum energetic electron precipitation (EEP)-OH impact. Hence, MLS is predominantly observing a lagged and lower estimate of the response of O_3 to EEP-OH at SZA > 95°. The EEP impact region within the TOM is smaller than the overlap region, strongly modulated by the background atmospheric dynamics. The results, although limited by the satellites viewing conditions, imply that the importance of EEP upon O_3 mixing ratio is strongly influenced by the background atmosphere, both in terms of chemistry and dynamics. Multisatellite observations at different solar local times are required to separate the direct from the lagged EEP-OH impact on O_3.

1. Introduction

In the high-latitude nighttime winter mesosphere, a local ozone (O_3) maximum is formed at high solar zenith angles (SZAs) near the polar night terminator at ~72 km. Marsh et al. (2001) called this maximum the tertiary ozone maximum (TOM). It owes its existence to the grazing incidence of solar radiation, leading to absorption and subsequently attenuation of radiation of wavelengths below 185 nm that photodissociate water vapor (H_2O) (see also Sonnemann et al., 2006). This in turn leads to absence of odd hydrogen (HO_X: H, OH, HO_2) production at the polar night terminator region, slowing down the catalytic cycles that destroy O_3. O_3 production, however, continues as the atmosphere is optically thin to wavelengths that dissociate molecular oxygen (O_2), which subsequently leads to formation of O_3. The absence of HO_X together with O_3 production leads to accumulation of O_3, which persists throughout the polar night (see, e.g., Aikin & Smith, 1999).

The lifetimes of O_3 in the vicinity of the TOM are in transition, ranging from >10 days below 70 km to about 0.01 day at 75-km altitude (see Smith et al., 2009). Depending on the lifetime of mesospheric O_3 during the polar night, this O_3 may be susceptible to dynamics. As such, the temporal and spatial distribution of the TOM is reported to be modulated by the gravity wave-driven mean meridional circulation pattern, with features that vary from year to year (e.g., Damiani et al., 2010; Smith et al., 2009, 2018; Sofieva et al., 2009). In addition, dynamical processes driven by planetary wave activity are known to cause downwelling of polar air. Periods of strong downwelling are observed more often in the Northern Hemisphere (NH) winters than in the Southern Hemisphere (SH) winters and are associated with sudden stratospheric warmings. The warming of the stratosphere gives a corresponding cooling in the mesosphere, after which there is warming in the mesosphere due to the adiabatic downward motions of air. Downwelling can either increase or decrease the O_3 density (see Smith et al., 2018). An increase in O_3 can be achieved through the descent of dry air (low H_2O), implying reduced production of HO_X through photolysis of H_2O, hence reduced O_3 loss through HO_X catalytic cycles, which in turn lead to accumulation of O_3. On the other hand, a decrease in O_3 can occur in two ways: Based on photochemistry, high temperatures imply reduced production of O_3, and the descent of the nighttime OH (hydroxyl radical) layer can lead to catalytic loss of O_3 provided there is sufficient atomic oxygen.

The distribution of the TOM is also modified by energetic particle precipitation (EPP) through solar proton events (SPEs) and energetic electron precipitation (EEP) events. Precipitating energetic particles produce odd nitrogen (NO_X) and HO_X chemical species that catalytically destroy O_3 (e.g., Crutzen & Solomon, 1980; Rusch et al., 1981; Solomon et al., 1981). The catalytic cycles involving HO_X species, however, predominate throughout the mesosphere, while NO_X catalytic cycles are most important in the stratosphere. The EPP-driven HO_X effects on mesospheric O_3 have been long studied through simulations/modeling even before observations of OH were available (e.g., Crutzen & Solomon, 1980; Solomon et al., 1983; Thorne, 1980). With the availability of OH and O_3 observations from Aura microwave limb sounder (MLS), several studies have confirmed the SPE-HO_X link to mesospheric O_3 depletion (e.g., Damiani et al., 2008; Seppälä et al., 2006; Sofieva et al., 2009; Verkhoglyadova et al., 2015, 2016). With the Aura MLS, a number of studies have also confirmed the importance of EEP on OH (e.g., Andersson et al., 2012, 2014b; Verronen et al., 2011; Zawedde et al., 2016, 2018). The impact of EEP on O_3 is, however, typically investigated without simultaneous OH measurements.

MLS monitors both O_3 and OH and hence allows for a unique opportunity to study whether the apparent O_3 changes are correlated with OH. Moreover, there are scarcely any studies that observe EEP, OH, and O_3 simultaneously and hence could verify that the changes observed in O_3 are due to OH enhancement produced by EEP and not a change related to, for example, dynamics.

Apart from the EEP forcing and the highly dynamic wintertime modulating O_3, there are limitations due to chemistry in that O_3 takes place in the presence of atomic oxygen which is mainly abundant during sunlit hours when it is produced by photodissociation of O_2 (see, e.g., Aikin & Smith, 1999; Thorne, 1980; Turunen et al., 2016; Verronen et al., 2013). This imposes limitations on the SZA at which O_3 reduction takes place. Further, the region of electron precipitation (auroral zone) should coincide with the TOM. Hence, to monitor the direct EEP-OH effect on O_3, the satellite must make observations at the SZA (or local times) at twilight, either in the morning or evening when the wintertime TOM exists and there is abundant atomic oxygen to allow catalytic O_3 reduction (see also Turunen et al., 2016). Observations that do not overlap with the auroral zone, TOM and sunlit or twilight conditions will be affected by the lifetime of OH and recovery time of O_3. Hence, observing an O_3 decrease during nighttime implies that the catalytic reduction has taken place earlier at the polar night terminator. Lack of decrease during an EPP event may indicate that the potential O_3 reduction has not yet occurred due to lack of photolysis and atomic oxygen. During daytime, however, the O_3 reduction by EPP is hard to detect as the sunlight destroys O_3 efficiently, and an additional source would not be prominent.

In this study, we investigate when the overlap between the TOM and the auroral zone exists using Aura MLS O_3 observations for years 2005–2006. We identify the time and spatial locations at which EPP, and in particular EEP, may be important for the TOM. With particle observations from the National Oceanic and Atmospheric Administration/Polar Orbiting Environmental Satellites (NOAA/POES) Medium Proton and Electron Detectors (MEPED) 0° and 90° telescopes, we further explore the effects of EEP-OH on the TOM for the same period of time. By selecting two pairs of EEP events and SPEs during the same wintertime conditions (same month), we study the relative importance of EEP events and SPEs. We also use MLS H_2O mixing ratio observations to evaluate the efficiency of the EPP-OH production, as well as temperature to monitor the vertical motion of air, in correlation analysis focusing on January 2005 and December 2006. Finally, a superposed epoch analysis is applied identifying EEP events occurring exclusively in the winter months of years 2005 to 2009, evaluating the response on OH and O_3 mixing ratios simultaneously. The aim is to understand potential cavities of using the MLS observations related to the EPP-OH impact on the TOM in order to better assess the potential role of EPP as a driver in the Earth's atmosphere.

2. Data

2.1. Aura MLS Observations

The MLS instrument on board the National Aeronautics and Space Administration (NASA) Aura Satellite measures naturally occurring microwave thermal radiation from the limb of Earth's atmosphere to remotely sense vertical profiles of atmospheric constituents (Schoeberl et al., 2006; Waters et al., 2006). In this study, we use Aura/MLS observations of the atmospheric constituents: temperature, H_2O, OH, and O_3

mixing ratios (version 4.2x–1.0) for years 2005 to 2009 in the NH, sorted as described in the data quality and description document (Livesey et al., 2015).

The OH background density is low during nighttime, making EPP-related changes in OH easily detectable at night. Hence, similar to Andersson et al. (2014a), we use SZA > 95° to include also observations under twilight conditions since catalytic destruction of O_3 requires atomic oxygen that is only abundant under sunlit conditions. Moreover, the HO_X chemical life time is of the order of hours in the region of interest, the mesosphere (Pickett et al., 2006), hence OH is not significantly influenced by transport. The temporal, vertical, and horizontal resolution of OH in the mesosphere is 25 s, 2.5 km, and 165 km, respectively. For temperature, H_2O, and O_3, the vertical and horizontal resolutions are coarser and vary within the mesosphere (62–75 km) (see Livesey et al., 2015).

2.2. NOAA/POES Observations

The MEPED 0° and 90° telescopes which are part of the space environment monitor-2 instruments on board the NOAA/POES satellites provide measurements of fluxes of trapped and precipitating particles. For year 2005, we use particle data from NOAA-16 while for years 2006 to 2009, particle data from NOAA-18 are utilized because these two satellites measure particles that are closest in time and space to the atmospheric observations made by the Aura satellite.

The MEPED electron data are known to be contaminated by low-energy protons, while the solid state detectors of the proton telescope are affected by degradation due to radiation damage (Evans & Greer, 2000). The procedures for correcting the MEPED electron data are described in Nesse Tyssøy et al. (2016). Using the correction factors derived by Sandanger et al. (2015) and Ødegaard et al. (2016), the proton fluxes are corrected for radiation damage before they are used to correct the electron data from proton contamination. The new optimized geometric factors lead to new electron channels energy thresholds as follows: >43 keV, >114 keV, >292 keV, and >756 keV (Ødegaard et al., 2017), of which the fourth channel is obtained from relativistic electrons contamination of the P6 channel of the proton telescope detectors (Nesse Tyssøy et al., 2016).

With an anisotropic distribution of particles, with decreasing fluxes toward the center of the loss cone, the 0° and 90° telescopes tend to either underestimate or overestimate the fluxes of the precipitating particles, respectively (Nesse Tyssøy et al., 2016; Rodger et al., 2010, 2013). Therefore, using a combination of measurements from the 0° and 90° telescopes together with electron pitch angle distributions from the theory of wave-particle interaction, a complete bounce loss cone flux is derived for each of the electron energy channels (Nesse Tyssøy et al., 2016). A monotonic piecewise cubic Hermite interpolating polynomial (PCHIP) (Fritsch & Carlson, 1980) is fitted to the integral fluxes which, thereafter, are converted into a differential electron spectrum (43–756 keV). The procedure, which is described in Nesse Tyssøy et al. (2016), includes calculating the number of electrons per second that pass through a horizontal surface of size 1 cm^2 at 120-km altitude. We then find the isotropic flux that gives the same number of electrons per second passing through this unit horizontal area, which we refer to as the equivalent isotropic flux level over the bounce loss cone. Each energy interval is treated separately as the level of diffusion will depend on the particle energy. The energy deposition as a function of altitude is then calculated by using the differential electron spectrum and the results of the Rees (1989) model, taking into account the cosine factor that enters when converting from flux to particles passing through a horizontal unit surface. In these calculations we have used the COSPAR (COmmittte on SPAce Research) 1986 Reference Atmosphere.

The proton fluxes used are a combination of measurements from the MEPED proton 0° telescope which measures the proton fluxes with energies >30 keV to >6,900 keV and the omnidirectional 0–60° detectors that measures the proton fluxes with energies >16 MeV to >70 MeV (see Nesse Tyssøy & Stadsnes, 2015; Nesse Tyssøy et al., 2013). At high latitudes, both the 0° detector and the omnidetector measure protons in the loss cone, and isotropic fluxes are expected during SPEs. By fitting PCHIP to the measurements from both detectors, integral spectra are obtained from which the energy deposition height profiles are calculated based on the range energy of protons in air given by Bethe and Ashkin (1953). The atmospheric densities are retrieved from the MSIS-E-90 model (Hedin, 1991). We include the SPEs of >1,000 particle flux units for energies >10 MeV (https://umbra.nascom.nasa.gov/SEP/), during 2005 and 2006 presented in Nesse Tyssøy and Stadsnes (2015).

10.1029/2018JA026201

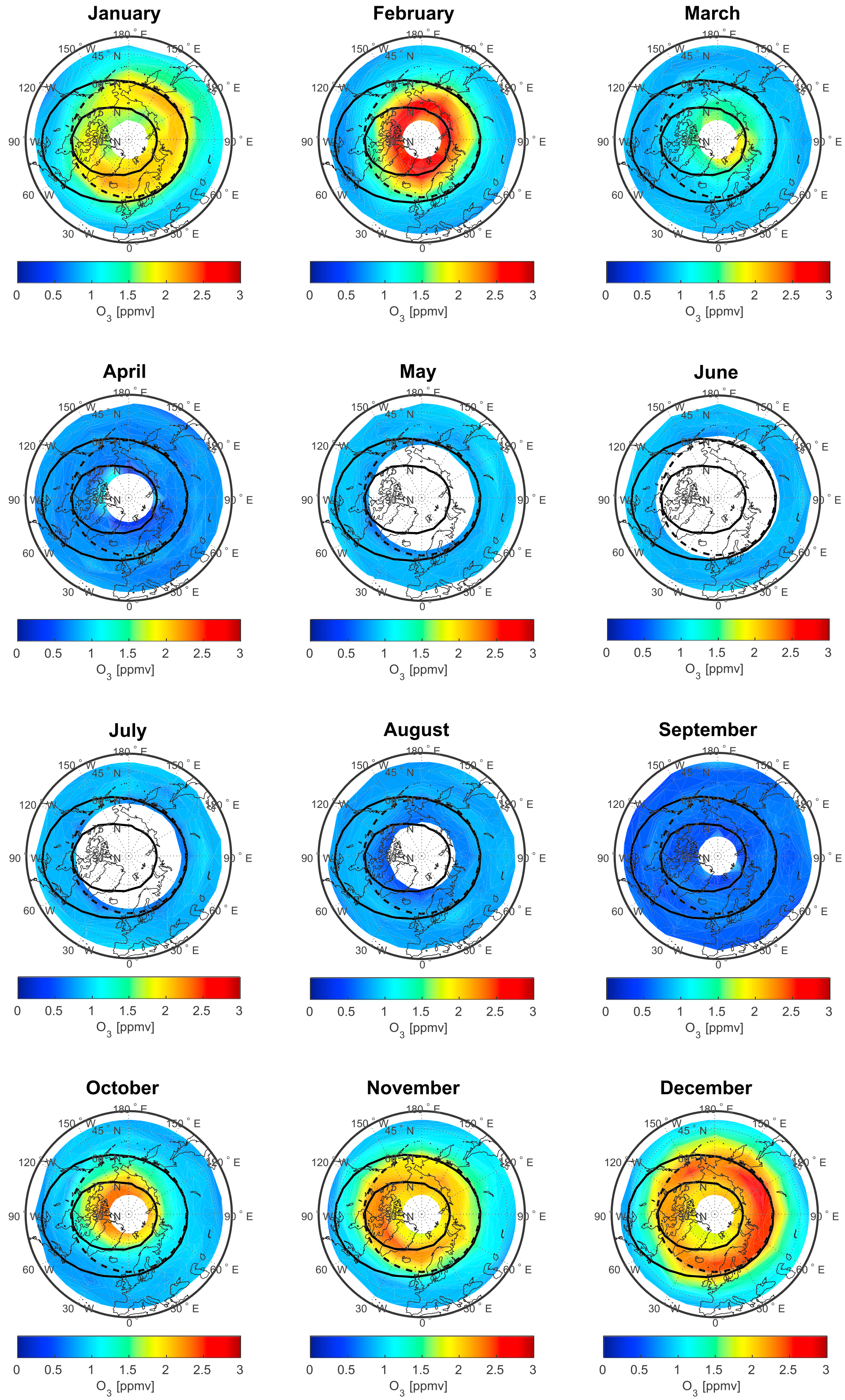

Figure 1. Overview maps showing monthly averaged nighttime O_3 at 75 km for January to December 2005 for solar zenith angle > 95° in the Northern Hemisphere. Mean values were calculated for each 5° latitude by 20° longitude bin between latitudes 40°–80°N and longitudes 180°W to 180°E. The black solid oval lines show the approximate locations of 55°N and 70°N corrected geomagnetic latitude, hence the latitude extent of the auroral zone or the footprint of the outer electron radiation belts. The black dashed lines represent the geographic latitude 60°N.

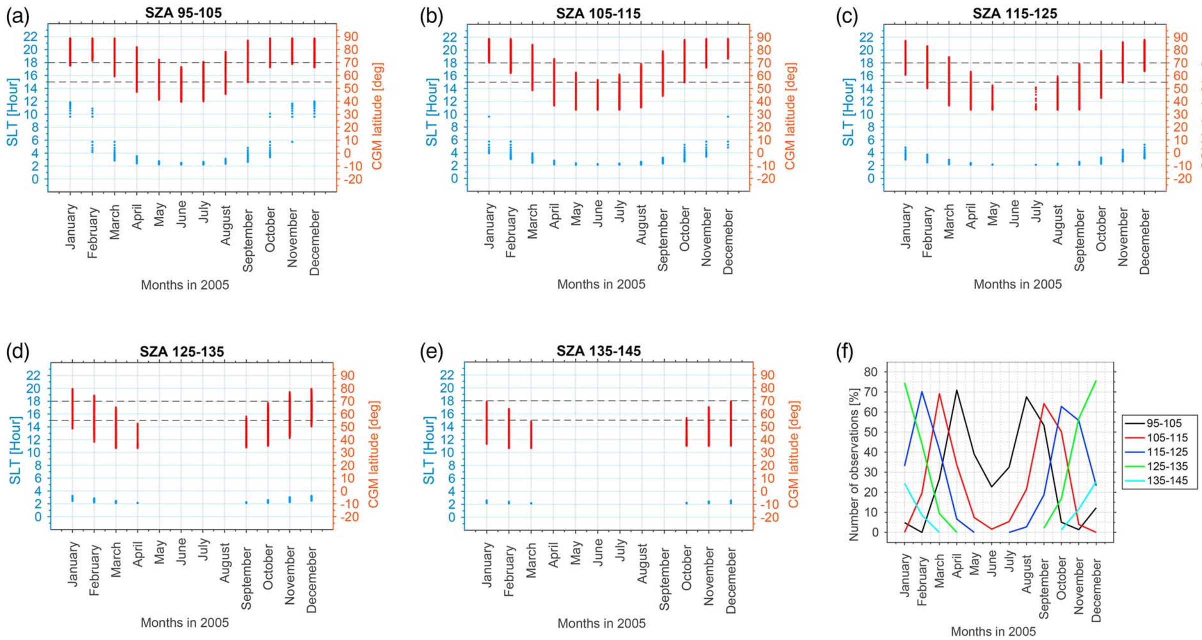

Figure 2. (a–e) Plots showing the SLT and CGM latitude coverage for O_3 observations over different SZA bands for the geographical latitude band of 40°–80°N during the months of year 2005. The horizontal black dashed lines denote the CGM latitudes 55° and 70°N. (f) The number of observations taken within the auroral zone at the different SZA bands, expressed as a percentage of the total number of observations taken within the latitude band 40°–80°N during each month of year 2005. SLT = solar local time; CGM = corrected geomagnetic; SZA = solar zenith angle.

3. Methods and Results

In this study, we focus on twilight-nighttime O_3 mixing ratios at altitudes (67, 70, and 75 km) in the vicinity of the TOM in the NH. For all maps in this study, mean values are calculated for each 5° latitude by 20° longitude bin between latitudes 40°–80°N and longitudes 180°W to 180°E. The data set is further sorted into five classes (or bins) based on the SZA: 95°–105°, 105°–115°, 115°–125°, 125°–135°, and 135°–145° in order to differentiate between the direct and lagged O_3 impact. Note that the term "direct O_3 response" implies O_3 loss during the period and at the location of precipitation. While the term “lagged response” refers to O_3 loss due to EEP-induced HO_X, after the precipitation has occurred since HO_X can stay for 0.1–1 day after production in the mesosphere (Pickett et al., 2006). After the HO_X and rates of the HO_X catalytic cycles recover to normal values, the odd oxygen (O_X: O, O_3) production during sunlit hours results in almost complete O_X recovery by noontime of the next day (Turunen et al., 2016). Some modeled and observational studies show that the atmosphere (OH and O_3) recovers from EPP impact 2–3 days after the end of the EPP event (see, e.g., Damiani et al., 2008; Jackman et al., 2011; Seppälä et al., 2006; Verronen et al., 2006). However, to allow for complete O_3 recovery, we assume that quiet-time level is reached at 4 days after the end of a particle precipitation event.

3.1. When Is There Overlap Between the Tertiary Ozone Maximum and the Auroral Zone?

Figure 1 shows the evolution of the monthly mean nighttime O_3 mixing ratios at 75-km altitude throughout the year 2005 in the NH. The approximate location of the corrected geomagnetic (CGM) latitude band 55°–70°N where EEP is expected, is indicated by the black oval lines, hereafter referred to as the auroral zone. O_3 mixing ratio enhancements of approximately 1.5–3 ppmv around the geographic pole are seen in January to March and October to December. This is the TOM. It exhibits maximum extent in latitude, extending equatorward to latitudes below 60°N (dashed lines) during January and December 2005 in the NH. The same months exhibit the largest region of intersection (60°–120°W) between the auroral zone and the TOM at 75-km altitude. For February and November, the region of intersection is less as the extent of the TOM is poleward of 60°N. During March and October, the O_3 mixing ratio is lower and the region of intersection is also smaller. The SZA distribution should be symmetric around winter solstice on 21 December. This means that the month October should on average have more nights with greater SZA than the month March. From April to September, the TOM does not exist. The O_3 mixing ratio is less than 1 ppmv and for large parts of the polar cap (during May–July) there are no measurements at SZA > 95°.

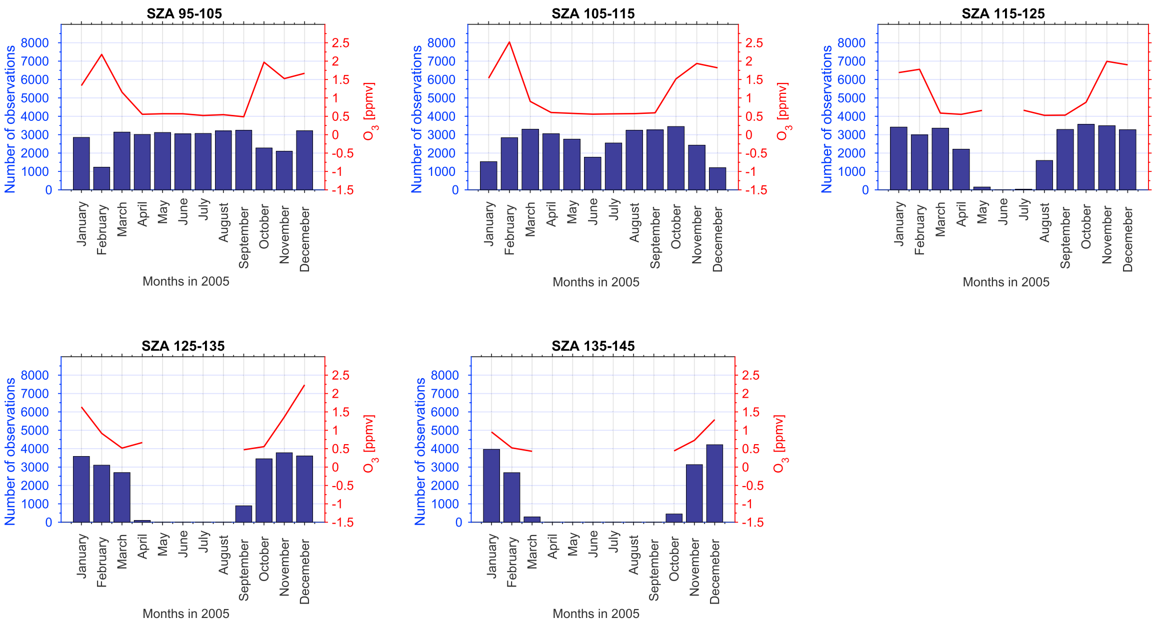

Figure 3. The red line shows the monthly averaged O_3 at 75 km over the different solar zenith angle (SZA) bands for the geographical latitude band of 40°–80°N during the months of year 2005. The blue bar plots show the number of observations in each monthly mean respectively.

Assuming that the role of O_3 in the mesospheric energy budget is proportional to its volume mixing ratios, the impact of EPP is potentially larger if it takes place in the region of the TOM. Further, the catalytic reactions require the presence of sunlight that photodissociates O_2 to produce atomic oxygen. Figure 2 shows the solar local time (SLT) (blue) and CGM latitudes (red) at which MLS-O_3 observations are made at the five SZA bands (95°–105°, 105°–115°, 115°–125°, 125°–135°, and 135°–145°) during the months of year 2005. Also shown in Figure 2f is the number of observations within the auroral zone at each SZA band expressed as a percentage of the total number of observations during each month of year 2005. For the 95°–105° SZA band (black line in Figure 2f) which coincides with morning hours, there are few or no O_3 measurements (0–12%) taken during midwinter months January–February and November–December within the auroral zone. This implies that Aura/MLS barely observes the direct reduction of O_3 by HO_X during the winter months. At other months (March–September) when the TOM does not form, there are more measurements (23–71%) within the precipitation zone. The same behavior is seen for the SZAs 105°–115° band (red), which is nighttime, with decreasing measurements during summer months.

Figure 3 shows the monthly mean O_3 mixing ratio at 75 km for the five SZA bands, together with the number of measurements comprising each monthly mean. For the 95°–105° SZA band, maximum O_3 mixing ratio (about 2.2 ppmv) are seen in February, followed by October–December (about 2.0 ppmv) and January (about 1.4 ppmv). There is a trough between March to September with a minimum value of about 0.6 ppmv. The same kind of behavior is seen for the SZA band of 105°–115°. For the rest of the SZA bands (115°–145°), O_3 mixing ratio during winter months generally reduce with increasing SZA. During the summer months, the data coverage becomes poorer with increasing SZA.

Figure 1 shows that considering all SZA > 95°, the TOM exhibits maximum overlap with the auroral zone during the months of January and December 2005. When the data are sorted by the different SZA bands, however, the situation is quite different as there are fewer observations within the auroral zone for the SZA band of 95°–105°, which corresponds to twilight hours during January and December 2005. At twilight, the TOM formation can take place as well as photodissociation of O_2 from which atomic oxygen forms, which is required for efficient catalytic removal of O_3. During polar night conditions, the evening twilight O_3 density will be maintained (constant) throughout the night (see, e.g., Aikin & Smith, 1999; Sofieva et al., 2012, 2009, and references therein). Since there is limited overlap between the TOM and the auroral zone at twilight conditions, the MLS observations will predominantly show the lagged O_3 response to EEP-OH within the auroral zone for SZAs > 95°. The 95°–105° and 105°–115° SZA bands in Figure 3 show an O_3 reduction in January, which is also evident in Figure 1. This O_3 reduction corresponds to the January 2005 SPE

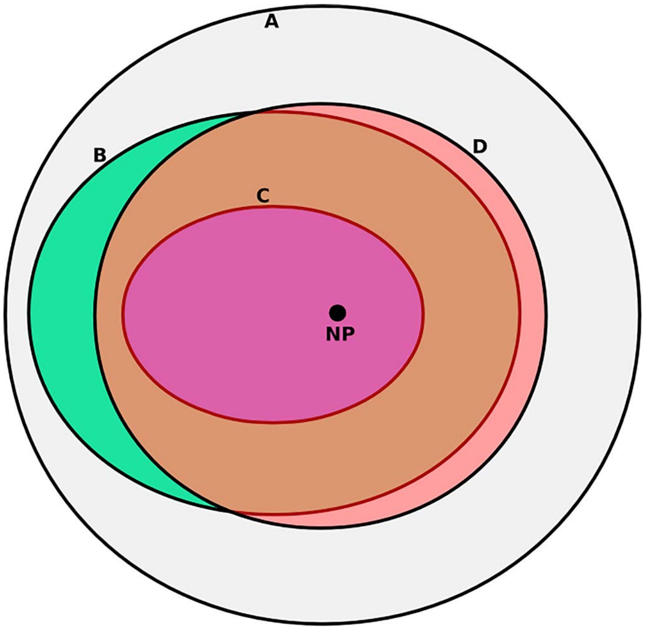

Figure 4. A schematic diagram showing the overlap between the tertiary O_3 maximum (TOM) and the auroral zone where electron precipitation is expected in the Northern Hemisphere. This overlap is the region shown in color brown. The region in green represents the part of the auroral zone that does not coincide with the TOM. Whereas the regions marked by red and magenta represent parts of the TOM that do not coincide with the auroral zone. (A) Outer boundary when looking down on the Northern Hemisphere, for example, latitude 40°N. The acronym NP represents the geographic North Pole. (B) The corrected geomagnetic latitude 55°N. (C) The corrected geomagnetic latitude 70°N. (D) The latitude extent of the TOM, defined based on the O_3 distribution of December 2005.

(see, e.g., Damiani et al., 2008; Seppälä et al., 2006; Verronen et al., 2006), and the January 2005 EEP events. The other SZA bands (115°–145°) that exhibit maximum overlap with the auroral zone do not exhibit a similar O_3 reduction in January.

A schematic of the geographical overlap between the TOM and the auroral zone is illustrated in Figure 4 by the brown region. The magenta and red regions are parts of the TOM that do not coincide with the precipitation zone, while the green region is part of the oval that does not coincide with the TOM. The letters B and C represent the CGM latitudes 55°N and 70°N, respectively, while D is the latitude extent of the TOM. The direct EEP-OH driven O_3 reduction is expected within the brown region during twilight, but measurements must also take place at the same time within that region to allow for direct observations of this effect. Otherwise, measurements taken at higher SZAs in that geographical region would detect the lagged effect of EEP-OH on O_3.

3.2. Case Studies of the Effects of EPP-OH on the Tertiary O_3 Maximum

To study the effects of EEP-OH on the TOM in comparison to SPEs during the same wintertime conditions, the months January 2005 and December 2006 are selected, during which there are both SPEs and EEP events. As pointed out in section 3.1, these are the same months when the TOM exhibits maximum overlap with the auroral zone. The SPEs periods are selected based on the list of SPEs (https://umbra.nascom.nasa.gov/SEP/) with >1,000 particle flux units. EEP periods are selected based on the mean electron energy deposition at 75 km during the years 2005 to 2006 (not shown). Periods with electron energy deposition above the mean value are considered EEP events, while those with electron energy deposition below the mean value are considered quiet time. This gives six and five EEP days during January 2005 and December 2006, respectively. The quiet-time periods are each 5 days. Zawedde et al. (2018) show that OH variability is largely explained by the background or seasonal variations in temperature and H_2O. Therefore, to monitor the seasonal changes associated with the different events, observations of temperature and H_2O are included in the analysis.

The month of January 2005 starts with EEP events (2–7 January), followed by a SPE (16–23 January), and a quiet-time period (27–31 January). The mean nighttime energy deposition, OH, O_3, H_2O mixing ratios, and temperature at 75 km of which are shown in Figure 5. During the EEP event, the electron energy is deposited at all longitudes within the auroral precipitation zone, but significantly weaker in the sector 50°–0°W. It does not show a clear one-to-one relationship with the OH enhancements or with the O_3 reduction. During the SPE, the proton energy is deposited more homogeneously within, as well as poleward of the auroral zone. The corresponding OH enhancements exhibit structures that are not seen in the energy deposition. However, there is appreciable reduction in O_3 seen all over the geographic extent of the TOM, corresponding with the OH enhancement all over the polar cap, as well as the auroral zone. The quiet-time period exhibits some structures in OH mixing ratios within longitudes 180°W to 90°E, corresponding with low H_2O mixing ratios and high temperatures. The geographic coverage of the TOM is somewhat reduced in the quiet-time period due to seasonal effects (see Figure 1), but increased in intensity. There is also more O_3 in the region 60°W to 120°E, corresponding to low H_2O mixing ratios and high temperatures. This may be an indication of accumulation of O_3 due to low H_2O (low HO_X) mixing ratios, hence reduced catalytic loss of O_3. During quiet-time and SPE, the H_2O minima seem to be a bit out of phase with the temperature maxima.

The month of December 2006 starts with five days (1–5 December) of quiet-time period, followed by a SPE period (6–16 December) and then an EEP event (20–24 December) whose energy deposition, OH, O_3, H_2O mixing ratios, and temperature maps at 75 km in the NH are shown in Figure 6. Note that the EEP event starts a few days before 20 December, closely succeeding the SPE. To ensure, however, that we are showing only the effect of energetic electrons, we have applied a 4-day buffer period as described earlier in section

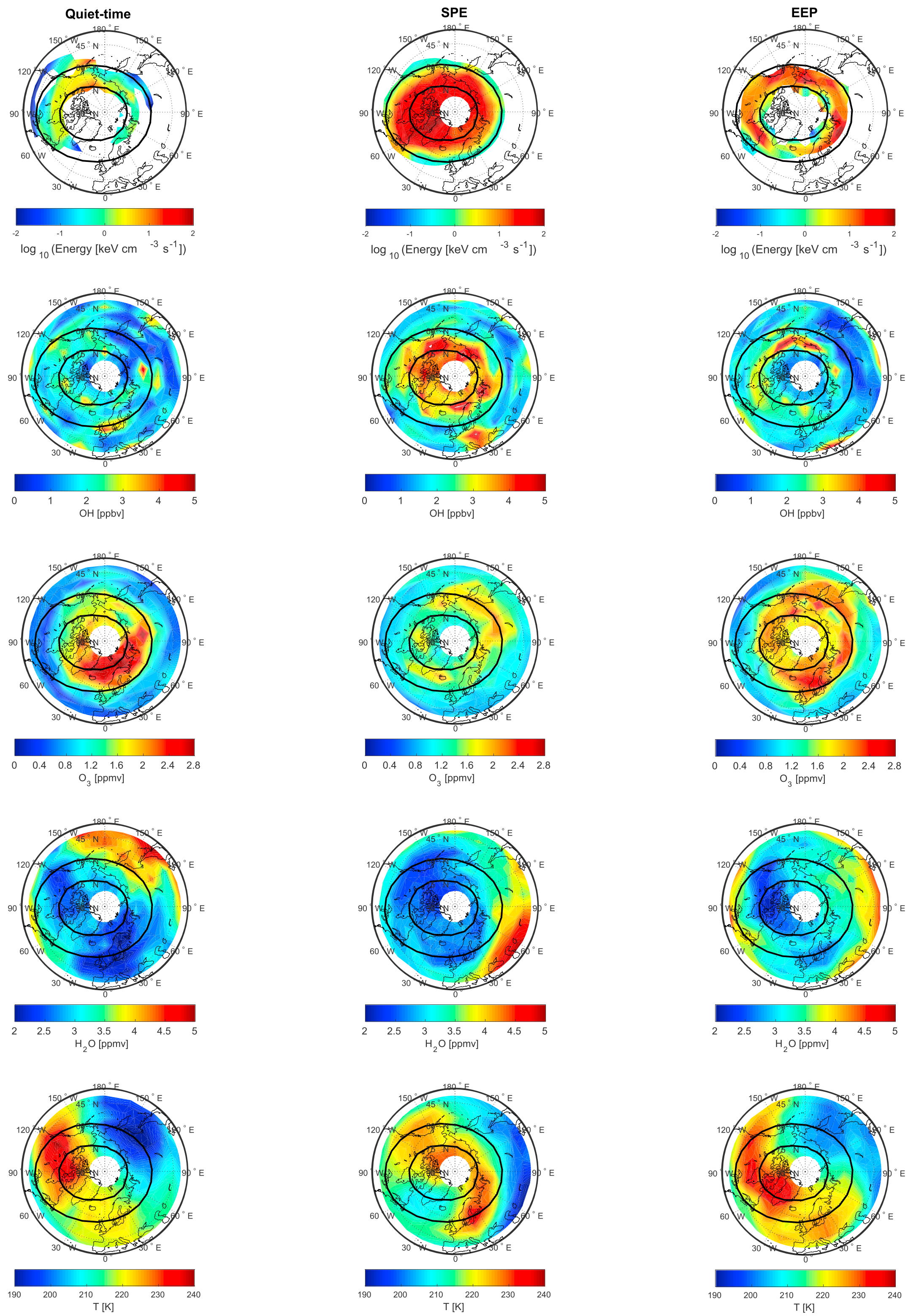

Figure 5. Mean nighttime distribution of energy deposition, OH, O_3, H_2O, and temperature for SZA > 95° at 75 km within the geographical latitude band of 40°–80°N during the months of January 2005 for EEP (2–7 January), SPEs (16–23 January), and quiet-time (27–31 January) periods. Mean values were calculated for each 5° latitude by 20° longitude bin between latitudes 40°–80°N and longitudes 180°W–180°E. The black oval lines show the approximate location of 55°N and 70°N corrected geomagnetic latitude. SZA = solar zenith angle; EEP = energetic electron precipitation; SPEs = solar proton events.

10.1029/2018JA026201

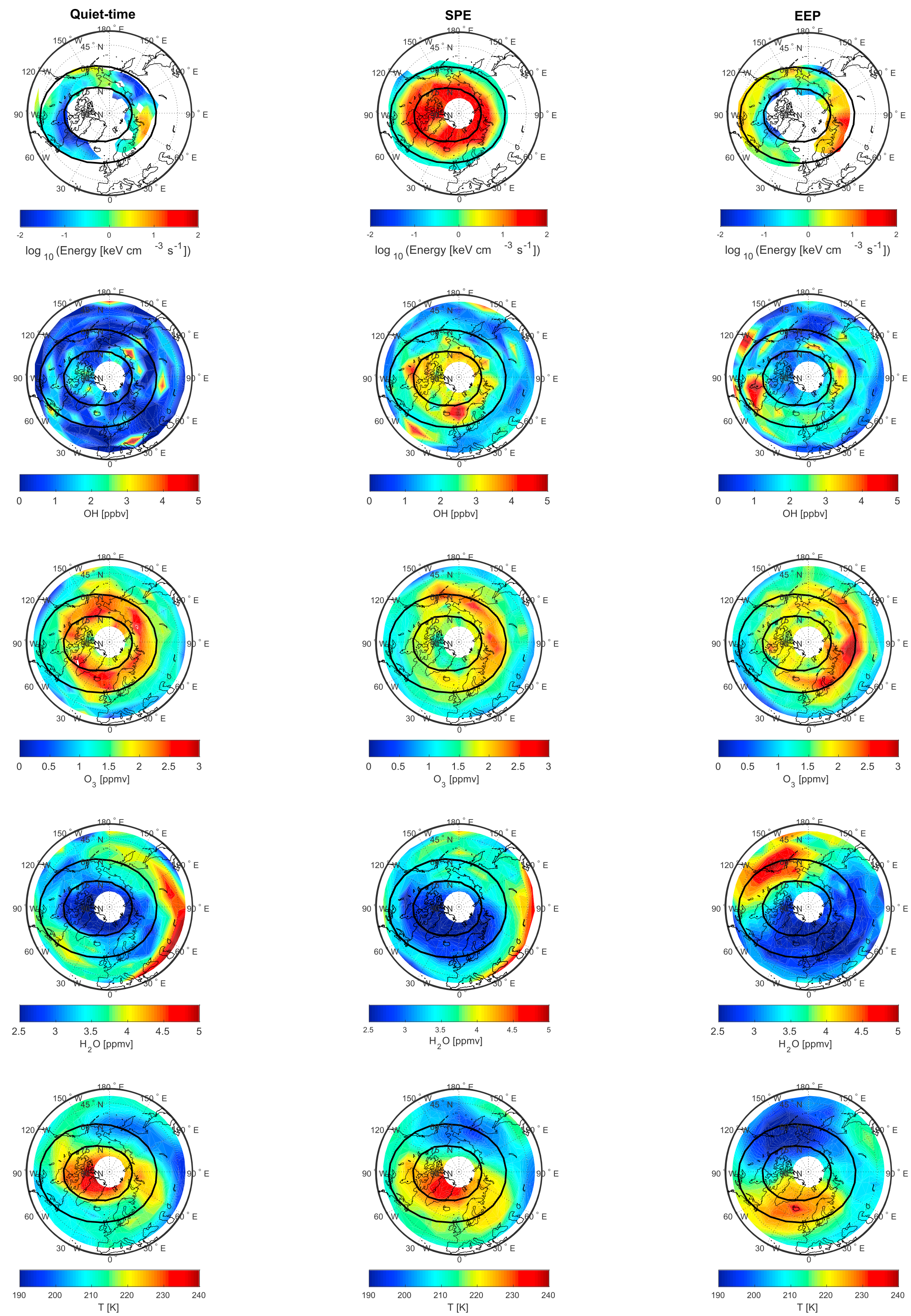

Figure 6. Mean nighttime distribution of energy deposition, OH, O_3, H_2O, and temperature for SZA > 95° at 75 km within the geographical latitude band of 40°–80°N during the months of December 2006 for quiet-time (1–5 December), SPEs (6–16 December) and EEP (20–24 December) events. Mean values were calculated for each 5° latitude by 20° longitude bin between latitudes 40°–80°N and longitudes 180°W to 180°E. The black oval lines show the approximate location of 55°N and 70°N corrected geomagnetic latitude latitude. SZA = solar zenith angle; EEP = energetic electron precipitation; SPEs = solar proton events.

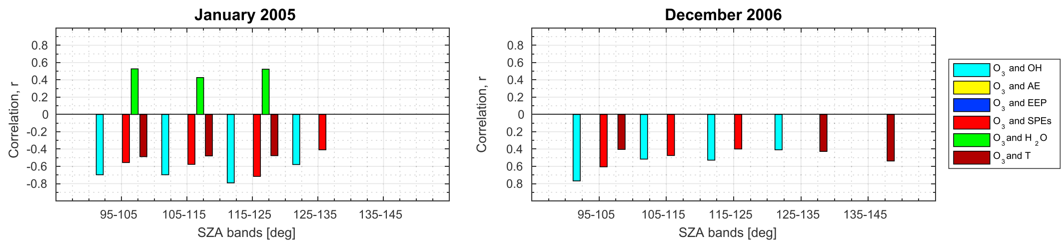

Figure 7. (Top) Correlation between daily mean O_3 and the daily means of OH, AE index, electron energy deposition, proton energy deposition, H_2O, and temperature for different SZA bands within the geographical latitude band of 40°–80°N for January 2005 (left) and December 2006 (right). The energy deposition, OH, and O_3 are averages at 75 km. Only the correlation deemed significant at 95% confidence interval (or p value <0.05) is shown. The p value is the random chance probability of getting a significant correlation when the true correlation is zero. SZA = solar zenith angle; EEP = energetic electron precipitation; SPEs = solar proton events.

3. The quiet-time period in this case exhibits, lower energy deposition and lower OH mixing ratio than that during January 2005. The tertiary O_3 extends a few degrees equatorward of the 60° latitude. During the SPE, the proton energy is deposited poleward of the 55° geomagnetic latitude, more intense toward the polar cap. Corresponding OH enhancement and O_3 reduction is seen all over the TOM. During the EEP event, the energy deposition exhibits two regions of enhanced values within longitudes 30°–90°E and 180°E to 60°W, with corresponding enhancements in OH mixing ratios. The O_3 reduction, however, seems to be modulated by EPP-OH, H_2O mixing ratio distribution, and the dynamics governing the temperature at this altitude. Generally, in this case the H_2O minimum correspond to temperature maximum.

3.3. Correlation Analyses for Two Winter Months

3.3.1. Correlation Analyses Based on Solar Zenith Angle

Spatially, there appears to be a negative correlation between the OH and O_3 mixing ratio during the SPE and EEP events in Figures 5 and 6. Due to the SZA dependence of OH and O_3, we proceed with correlation analysis based on the different SZA bands for January 2005 and December 2006. We calculate the daily means of the electron energy deposition, proton energy deposition, OH mixing ratio, O_3 mixing ratio, H_2O mixing ratio, and temperature at 75 km for the five SZA bands: 95°–105°, 105°–115°, 115°–125°, 125°–135°, and 135°–145°. The days with SPEs are excluded from the correlation of O_3 with EEP and the auroral electrojet (AE) index to exclude possible influence from SPEs. The daily mean AE index is included as a crude proxy for the EEP in case it is not captured by the single-satellite measurements of the electron fluxes.

To find out if there is a linear relationship between O_3 and each of the variables: OH mixing ratio, AE, electron energy deposition, proton energy deposition, H_2O mixing ratio, and temperature, we calculate Pearson's correlation coefficient, r, for all the five SZA bands at 75 km. The correlation analysis is performed on the time series for January 2005 and December 2006, the results of which are shown in Figure 7 (top) showing only the significant correlation. The correlation is deemed significant for p value < 0.05 (95% confidence interval). For January 2005, the variables OH, SPEs, H_2O, and temperature exhibit significant correlation with O_3 at SZAs between 95° and 135°, with maximum correlations of −0.79, −0.72, 0.53, and −0.49, respectively, occurring at the SZA bands of 115°–125° (for OH and SPEs) and 95°–105° (for H_2O and temperature). Both the AE index and EEP exhibit no significant correlation with O_3 at any of the SZAs. For December 2006, OH exhibits maximum correlation of -0.77 at SZAs 95°–105°, corresponding to twilight conditions. The H_2O, AE index, and EEP exhibit no significant correlation at any of the SZAs considered. SPEs exhibits maximum correlation (−0.60) at SZAs 95°–105°, corresponding to twilight conditions, decreasing in magnitude as the SZA increases, while temperature exhibits maximum correlation of −0.54 at SZAs 135°–145°.

The insignificant correlation of O_3 with EEP in both case studies may imply that EEP generally has no appreciable impact on the TOM. Reducing the number of observations (days) included in the correlation analysis when we remove days infested by SPEs might also play a part. The lack of correlation could, however, also be due to the viewing conditions of the MLS instrument. As shown in Figure 2, MLS is observing poleward of the auroral zone. This implies that the twilight region, where the direct O_3 reduction might occur does not coincide with the region with significant electron energy deposition. If a potential O_3 reduction is observed here at larger SZAs, it is related to EEP and OH produced in the auroral zone reducing the twilight O_3, and less O_3 is transported to these latitudes. In either case, it will not be correlated to the EEP energy

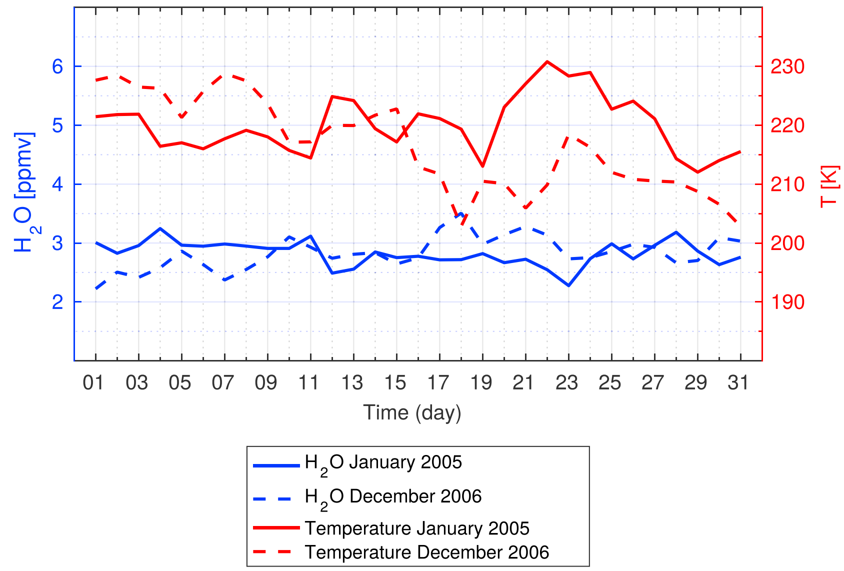

Figure 8. The daily mean H_2O (in blue) and temperature (in red) at 75 km for the solar zenith angle band of 95°–105° within the geographic latitude band of 40°–80°N. The plot for winter 2005 (January to March) is to the left while that of winter 2006 (October to December) is on the right.

deposited at these latitudes. At SZA > 115° the lack of atomic oxygen prohibit EEP-produced OH to effectively reduce O_3, hence, there is little correlation between EEP and O_3. SPEs are not limited to the auroral zone but impact the entire polar cap. Hence, MLS will observe SPE-produced OH in the presence of atomic oxygen and, subsequently, the direct impact on O_3.

There are peculiar correlation tendencies seen in Figure 7 in that during winter 2005, H_2O shows positive correlation with O_3 at SZAs between 95° and 135°, while during December 2006, the correlation between H_2O and O_3 is insignificant at SZAs 95° and 135°. This duality of H_2O might reflect its role in the photochemistry and in the dynamics. On a closer inspection of the H_2O daily mean mixing ratio for the SZA band of 95°–105°, Figure 8 shows that there is less variability in H_2O and temperature (up to 1.0 ppmv and 19 K) during January 2005 as compared to December 2006 (up to 1.25 ppmv and 26 K). Low H_2O mixing ratios as seen in both January 2005 and December 2006 reflect the downward air motions associated with the mean meridional circulation during winter, bringing down dry air, accompanied by adiabatic heating.

Downwelling can lead to lower O_3 production and hence a positive correlation between O_3 and H_2O (as seen in January 2005) in two ways: Based on photochemistry, higher temperatures imply lower production of O_3 and advection of air rich in HO_X can accelerate the catalytic loss of O_3 (see Smith et al., 2018, and references therein). On the other hand, downwelling can also lead to enhanced production of O_3 through decrease in H_2O and hence reduced HO_X production. This implies reduced O_3 loss by the catalytic reactions. This process, however, happens in phase with increased temperatures which predict lower O_3 production. Hence, the two processes counteract each other, leading to the insignificant correlation between O_3 and H_2O during periods that are highly dynamically perturbed as seen in December 2006. For detailed discussions on the variability of the TOM, see, for example, Smith et al. (2018).

In summary, SPEs exhibit significant correlation with O_3 at SZAs between 95° and 135°, corresponding to nighttime-twilight conditions over a wide geographic area. Both AE and EEP events exhibit no significant correlation with O_3 at all SZAs considered, for the two winters.

3.3.2. Correlation Analyses Based on the Geomagnetic Latitude Band

EEP events precipitate within a narrow band of CGM latitudes 55°–70°; hence, the effects thereof on OH and O_3 are expected within that band. By excluding days affected by SPEs, the Pearson correlation between O_3 mixing ratios and electron energy deposition is calculated at altitudes 67, 70, and 75 km within the CGM latitude band 55°–70°N (SZA > 95°) for January 2005, December 2006, and both January 2005 and December 2006. As before, the correlation is deemed significant for p values < 0.05. The correlation is insignificant at all altitudes during January 2005 and December 2006, except at 75 km during December 2006, which exhibits

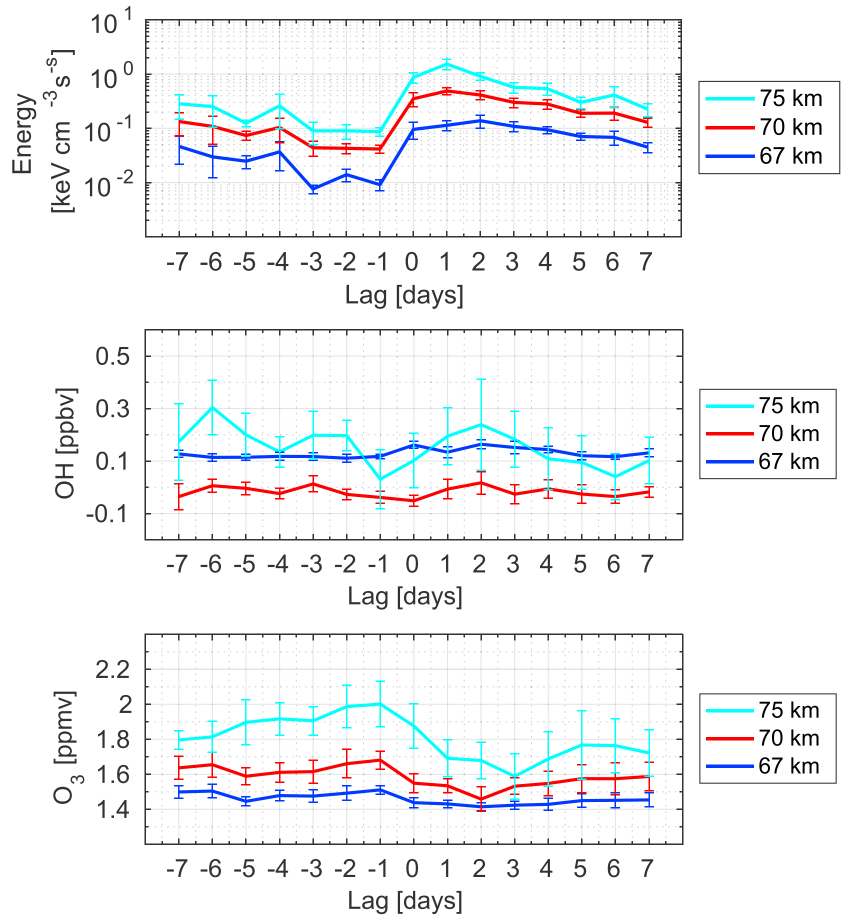

Figure 9. Superposed epoch analysis of the electron energy deposition, OH VMR, and O_3 VMR for energetic electron precipitation events during the winters of years 2005 to 2009 at altitudes close to the tertiary O_3 maximum (75, 70, and 67 km) in the corrected geomagnetic latitude band of 55°–70°N. The error bars represent the standard error of the mean.

a correlation coefficient of −0.8 (not shown). To increase on the sample size as well as occurrence of EEP, the correlation for December 2006 and January 2005 together is calculated. The correlation is insignificant at all altitudes even when both months are considered together.

The lack of a one-to-one relationship between EEP and O_3 within the auroral zone is probably due to the chemistry that depends on the SZA. The TOM forms at evening twilight, near the polar night terminator. The destruction of the TOM depends on the production of atomic oxygen during sunlit hours, which in turn depends on the SZA. Therefore, maximum intersection between the TOM and the production of atomic oxygen occurs during morning and evening (sunrise and sunset) hours; hence, efficient O_3 destruction occur there. The EEP-OH produced at other hours can start recovering before it can affect O_3, hence the mismatch between EEP increase and O_3 reduction (see Turunen et al., 2016). In this study, correlation analysis fails to show the EEP-OH relationship with O_3.

3.4. Superposed Epoch Analysis

Since correlation analysis has failed to unveil the impact of EEP-induced HO_X on the TOM, we opt for another method—composite analysis. Figure 9 illustrates a superposed epoch analysis of the electron energy deposition, OH and O_3 mixing ratios at altitudes close to the TOM (67–75 km) for 12 winter EEP periods (listed in Table 1) within the CGM latitude range of 55°–70°N for years 2005 to 2009. The standard error of the mean is represented by the dash-dotted lines. Days for which the daily mean energy deposition is greater than the 5-year mean are considered EEP periods. Zero lag refers to the first day of the EEP period that exceeds the limit (mean electron energy deposition). The periods with SPEs are excluded from this analysis. The electron energy deposition exhibits steady rises from lag zero day, peaking at lag 1 day for 70- to 75-km

Table 1
The List of EEP Events Based on the Energy Deposition at 75-km Altitude Within the CGM Latitude Band of 55°–70°N for the Winters of Years 2005 to 2009

Event	Date of EEP event
1	1–8 January 2005
2	11–15 January 2005
3	7–11 February 2005
4	26–28 January 2006
5	20–24 February 2006
6	18–31 December 2006
7	1–6 January 2007
8	17–28 January 2007
9	29 January to 9 February 2007
10	14–29 February 2007
11	5–11 January 2008
12	12–21 January 2008

altitudes, and at lag 2 days at 67-km altitude. The OH mixing ratio shows a rise from lag zero to a peak at lag 2 days for 67- to 75-km altitudes. The O_3 mixing ratio exhibits decreases at 67- to 75-km altitudes, with minima at lags 2–3 days. Hence, there is a lag of at least a day between the EEP-OH increase and the O_3 volume mixing ratio (VMR) reduction (see also Turunen et al., 2016). Note, however, that there might also be a seasonal bias in the events as they almost exclusively occur in January and February, hence there is likely a seasonal decrease in the O_3 mixing ratios time evolution.

To better estimate the change in O_3 mixing ratios at altitudes close to the TOM, Figure 10 shows the superposed epoch O_3 percentage change relative to a 7-days pre-events average for the 12 EEP events listed in Table 1. Also shown by the errorbars is the standard error of the mean. The maximum percentage decreases in O_3 are 16%, 9%, and 4% at 75-, 70-, and 67-km altitudes, respectively. The maximum decrease in O_3 mixing ratios at 75 km occurs on day 3. Whereas, at 70 and 67 km, the maximum decrease in O_3 mixing ratios occurs on day 2. This lagged behavior is already seen in Figure 9.

4. When and Where is EEP Important for the Tertiary O_3 Maximum?

Aura MLS provides a unique opportunity to study if an apparent O_3 change is associated with OH produced by EEP. In this paper we investigate time and spatial locations at which the EEP-OH effects on the TOM can be observed in order to better assess the EPP role on O_3 variability. We focus on the conditions and possible limitations of using Aura MLS O_3 observations in assessing the EEP-OH impact on O_3.

4.1. The General Formation and Sunrise Behavior of O_3 Mixing Ratios Observed by Aura/MLS

The TOM is formed near the winter polar night terminator (twilight conditions) at ~72 km at latitudes close to 60°, extending poleward covering the polar cap. At sunset, solar Ly-α radiation that is responsible for photolysis of H_2O is cut off first due to the grazing incidence (large SZA) of solar radiation near the polar night terminator, making the atmosphere opaque to Ly-α radiation. Therefore, production of HO_X species is cut off. The solar radiation in the Schumann-Runge bands have a much smaller O_2 absorption cross section than Ly-α has for H_2O (see Sonnemann et al., 2006). Thus, the production of atomic oxygen and hence O_3 increases in the absence of HO_X species. The high O_3 mixing ratios seen at SZA ~>95° in Figure 11, very prominent during quiet time, represent the TOM at 75 km within the latitude band 40°–80°N during January 2005 (top) and December 2006 (bottom). At SZA ~>130°, although still nighttime, the observations are progressively taken equatorward, away from the latitude range of the TOM as can be seen in Figure 12 (extreme right). This explains the low O_3 mixing ratios for SZA ≈>130° in Figure 11. Note that negative O_3 mixing ratios, as seen in Figure 11, stem from the fact that some of the MLS measurements have a poor signal-to-noise ratio for individual profiles. Any analysis that involves averaging will be biased if the points with negative mixing ratios are ignored (see Livesey et al., 2015).

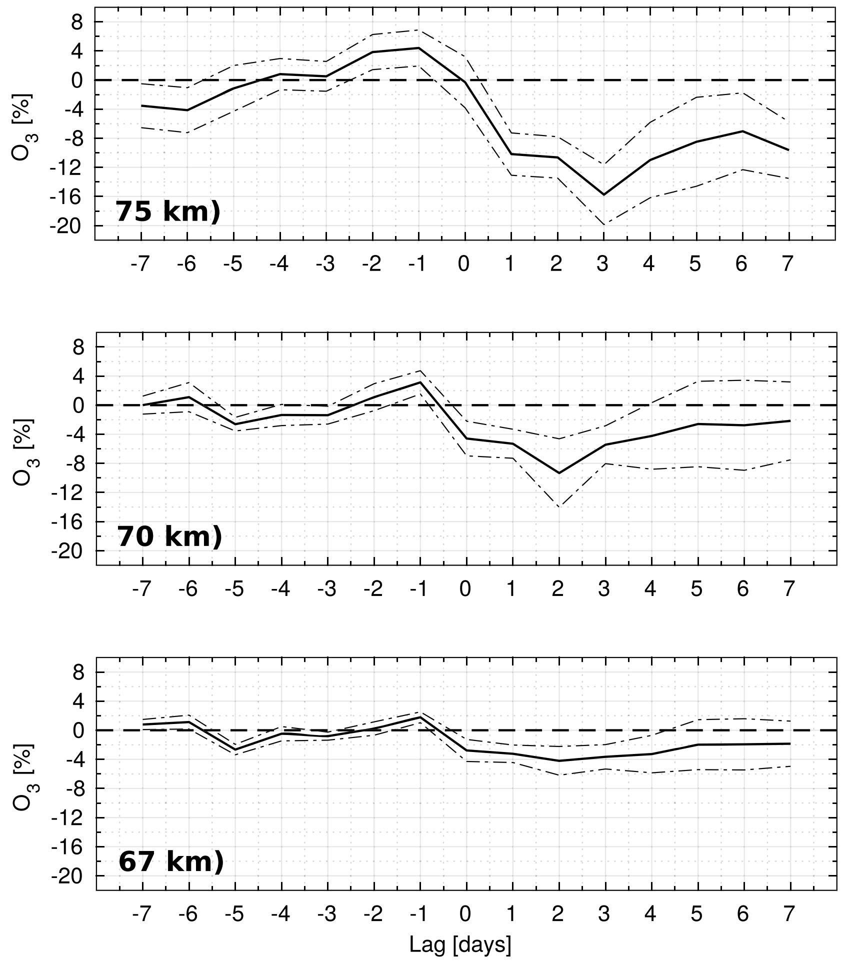

Figure 10. Superposed epoch analysis: The O_3 VMR percentage change relative to a 7-days pre-events average, for energetic electron precipitation events during the winters of years 2005 to 2009 at altitudes close to the tertiary O_3 maximum (75, 70, and 67 km) in the corrected geomagnetic latitude band of 55–70°N. The dash-dotted lines represent the standard error of the mean. The horizontal dashed lines represent the zero percentage change.

At sunrise, rapid photodissociation of O_3 by sunlight causes a rapid decreases in O_3 density. As solar ultraviolet radiation of wavelengths greater than the Schumann-Runge absorption of O_2 (200 nm < $\lambda \leq$ 240 nm) penetrates, the O_3 mixing ratio increases (Aikin & Smith, 1999). Although atomic oxygen is produced during this period, the efficiency of the catalytic cycles is low since production of HO_X species through photolysis of H_2O is reduced, hence the O_3 rise. Later as Ly-α radiation starts penetrating mesospheric altitudes, H_2O photolysis produces HO_X that catalytically destroys O_3, which is evident in Figure 11 at 80° < SZA < 100°. Rapid photolysis of O_3 leads to low concentrations during daytime (SZA < 80°).

4.2. The Conditions and Limitations for Observation of EEP-OH Effects on O_3

In Figure 4, the expected region of intersection between the precipitation zone and the TOM is represented by the brown region, which may vary in latitude coverage depending on the strength of the event and the seasonal extent of the TOM. The O_3 reduction occurs efficiently in the presence of abundant atomic oxygen that is required for the catalytic cycles. Although atomic oxygen is produced during EPP events, the amount formed by increased ionization is small compared to that produced by photodissociation (see, e.g., Aikin & Smith, 1999; Seppälä et al., 2006). Therefore, sunrise/sunset conditions are required for effective catalytic O_3 reduction (Turunen et al., 2016; Verronen et al., 2006). Moreover at sunrise, the O_3 production by photodissociation, which would balance the O_3 loss, is still relatively low compared to noon hours. At other hours, the concentration of the EEP-induced HO_X would decrease before it can affect O_3.

From Figure 1, it is clear that the maximum overlap between the oval and the TOM occurs during December–January in the NH winter. When the data are sorted by the five SZA bands, O_3 reduction is seen

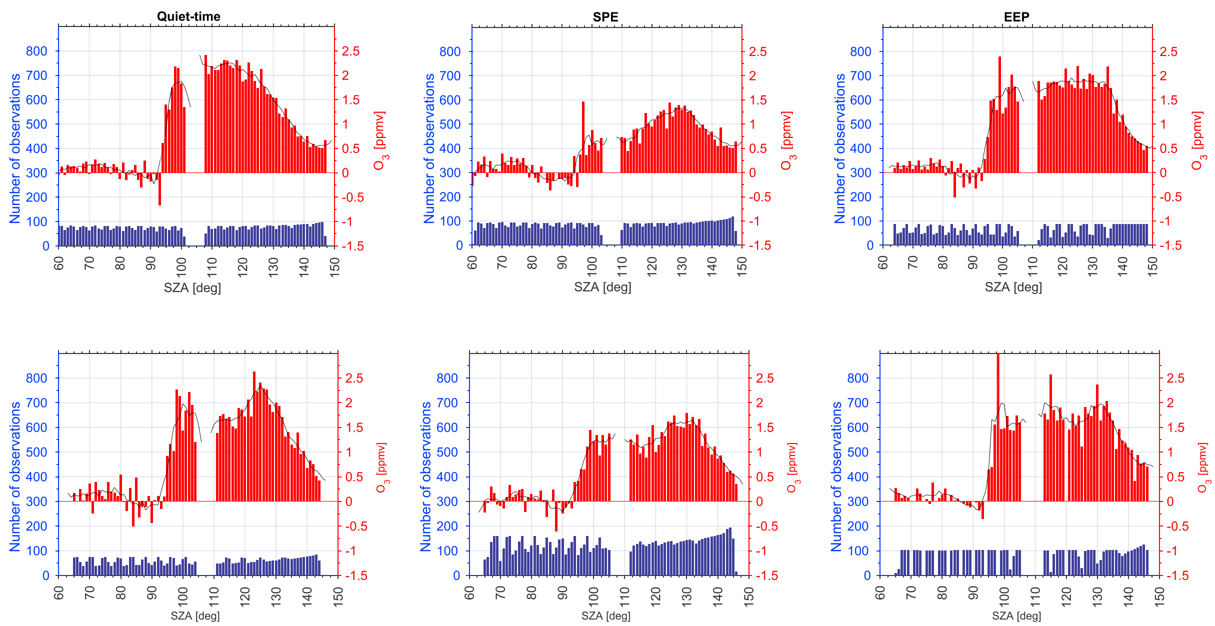

Figure 11. The variation of O_3 with SZA at 75 km within the geographical latitude band of 40°–80°N for January 2005 (top) and December 2006 (bottom). The red bars represent O_3 averages per SZA, calculated over the days during quiet-time, SPEs, and EEP periods. The black line represents the running mean of O_3 mixing ratios, averaged over a window of 5°. The blue bars represent the number of observations involved in the averages. SZA = solar zenith angle; SPEs = solar proton events; EEP = energetic electron precipitation.

in the month of January 2005 for SZA bands 95°–105° and 105°–115° in Figure 3. In December 2006, O_3 reduction extends from 95°–105° to 115°–125° (not shown). There is, however, very limited overlap between the O_3 measurements and the auroral zone during January and December for the SZA bands 95°–105° (morning twilight) and 105°–115° as seen in Figures 2 and 12. The intersection of the auroral zone with O_3 observations increases by the SZA band of 115°–125° and increases further with increasing SZA.

The Aura/MLS instrument mainly observes in the morning sector (SLT 2–13), covering the morning twilight within the geographic location 40°–80°N (see also Waters et al., 2006). For the January 2005 and December 2006 SPEs shown in Figure 11, reduction in nighttime O_3 is seen starting at SZA ~<135° as compared to the respective quiet-time periods. More reduction is seen at SZA ~<120°. This kind of behavior is also seen for the December 2006 EEP event, but not distinctly for the January 2005 EEP event. Since there is O_3 reduction prior to morning twilight conditions, it implies that an EPP source was active at or before evening twilight although the satellite was not at this location at evening twilight. Hence, MLS is observing a lagged effect of a potential EEP-OH impact on O_3. To observe the direct and hence maximum effect of EEP-OH on O_3, observations should be taken at twilight conditions, within the auroral zone during EEP events during wintertime when the TOM forms.

Further, based on Figures 5 and 6, it appears that electron precipitation is more effective in a region that is abundant in H_2O. H_2O is required for the formation of water cluster ions which are required in the process of EPP-OH formation (Solomon et al., 1981). The O_2^+ ion formed by ionization reacts with O_2, forming O_4^+ which uptakes H_2O, forming progressively larger water cluster ion at each stage of the reaction. The water cluster ions later dissociatively recombine with electrons forming H and OH (~2 HO_X per ionization). If the water cluster reactions are cut off by dissociative recombination with intermediates like O_4^+, then less than 2 HO_X per ionization are produced. This can occur if the H_2O mixing ratios reduce by a few parts per billion (pbb), then the natural electron concentrations may reduce the efficiency of EPP-HO_X production (Solomon et al., 1983). In recent study, Zawedde et al. (2018) report that H_2O is responsible for approximately 10% variability of OH mixing ratio at 75 km within geomagnetic latitudes 55°–70°N (auroral zone) for years 2005 to 2009, whereas the EEP contribution is 11%.

4.3. Observation of the Tertiary O_3 Maximum Within the Auroral Zone

Generally apart from the low O_3 mixing ratios during summer, there is restricted coverage by Aura MLS at high latitudes even though it covers parts of the auroral zone as shown in Figure 1. In this case, small changes

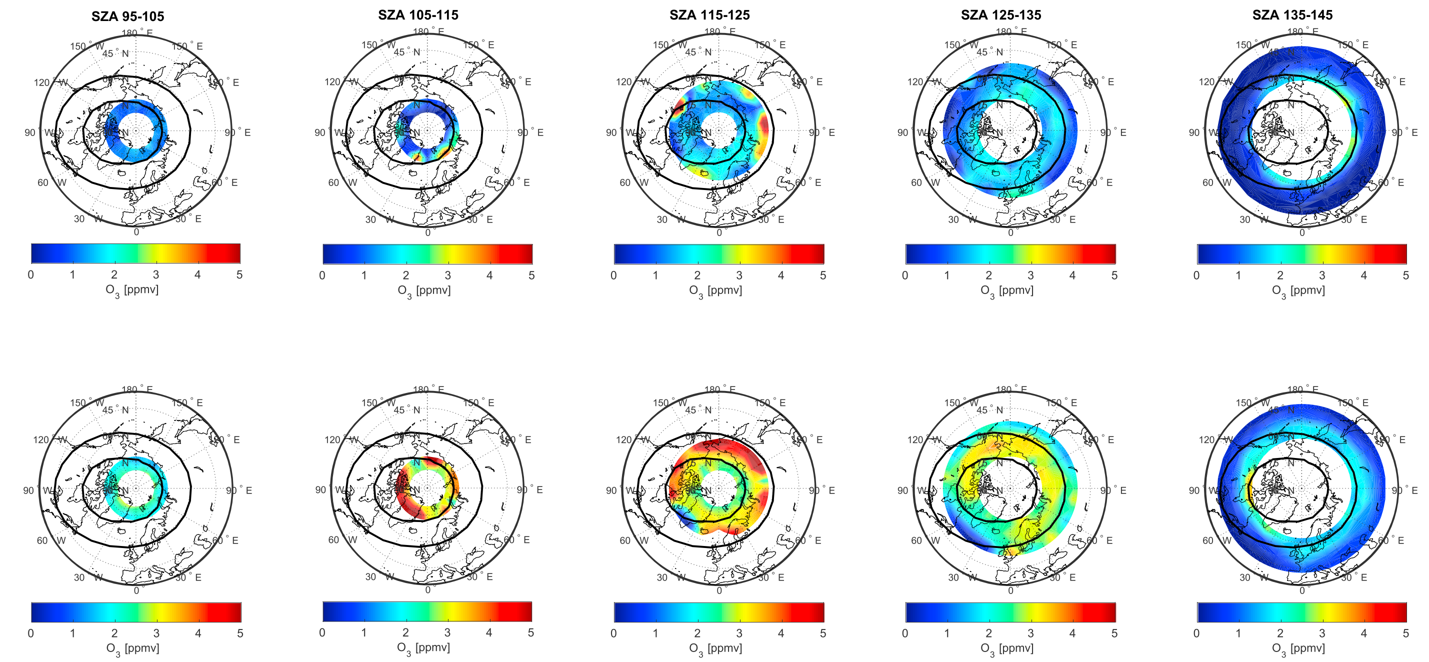

Figure 12. Monthly mean nighttime distribution of O_3 mixing ratio at 75 km for SZA bands between 95° and 145° within the geographical latitude band of 40°–80°N during January 2005 (top row) and December 2006 (bottom row). Mean values were calculated for each 5° latitude by 20° longitude bin between latitudes 40°–80°N and longitudes 180°W to 180°E. The black oval lines show the approximate location of 55°N and 70°N corrected geomagnetic latitude. SZA = solar zenith angle.

in the O_3 mixing ratios may result in large percentages that may portray a nonrealistic picture in regard to the EEP-OH impact on O_3. Therefore, in a statistical study, if there are more events during summer than during winter, the results normally expressed as anomalies may be biased by the summer large percentages. As such it seems more meaningful to perform the analysis in the winter hemisphere where there is abundant O_3 during nighttime as well as optimum intersection between the auroral zone and the TOM (see also Damiani et al., 2008, Figure 2).

Figures 5 and 6 show that during SPEs there is proton precipitation over the polar cap, extending to the auroral zone depending on the rigidity of the precipitating protons. There is corresponding OH enhancement. O_3 reduction is seen all over the latitude extent of the TOM, but most intense in regions with high temperatures/low H_2O mixing ratios, which in turn is modulated by planetary wave activity. High temperatures imply reduced production of O_3 based on photochemistry. Zawedde et al. (2018) show that SPEs contribute approximately 13% to the OH variability at 75 km within geomagnetic latitudes 55°–70°N (auroral zone) for years 2005 to 2009. In the same Figures 5 and 6, there is no clear one-to-one relation between the EEP-induced OH and the O_3 reduction as reduction seems to be in phase with the regions rich in H_2O, more evident in Figure 6. Planetary wave activity seems to be modulating the longitudinal distribution of H_2O at 75 km, hence modulating the longitudinal distribution EPP-OH which in turn modulates the distribution of O_3. H_2O is required for the formation of water cluster ions from which OH and H eventually form through dissociative recombination with electrons (see, e.g., Solomon et al., 1981). Of the EEP-OH formed, for example, in Figure 6, still only a portion lies within the geographic location of the TOM and can have an effect on O_3 in the presence of sunlight. Therefore, for this case, we see that only a portion of the energy deposition can eventually have an effect on the O_3 mixing ratios.

Although the impact region may seem rather small, it is important to find out if the frequently occurring EEP events would have a significant impact on nighttime O_3, and hence potentially important for the energy budget. Figure 7 shows the correlation of O_3 mixing ratio with the variables: OH mixing ratio, AE, electron energy deposition (EEP), proton energy deposition (SPEs), H_2O mixing ratio, and temperature separately for January 2005 and December 2006. The SZAs 95°–105° are considered to be under morning twilight conditions; therefore, the EEP-OH that has accumulated over a few hours and the direct EEP-OH will have drastic impact on the O_3 mixing ratios through catalytic cycles. This is possible when solar radiation that photodissociates O_2 penetrates the atmosphere to mesospheric altitudes. A modeling study by Turunen et al. (2016) also shows that for EEP occurring before sunrise, the largest relative change in O_X species is not seen during the electron forcing but after the HO_X catalytic cycles have had an impact in the morning.

EEP and AE exhibit insignificant correlation with O_3 at all SZAs considered. When the CGM latitude band of 55°–70°N (SZA > 95°) is considered, the EEP still exhibits insignificant correlation with O_3 at all altitudes considered, except at 75 km during December 2006. Therefore, by considering all SZA > 95°, most of the O_3 reduction we see, for example, in Figure 6 is predominantly that which was reduced at evening twilight and has not yet recovered. With Aura MLS, we can only observe little of the EEP-OH direct impact on O_3. This kind of limitation may also be present in some of the studies that have made the same SZA selection to study the EEP-OH direct effect.

The limitations are not as strict for SPEs since they precipitate over the entire polar cap, covering almost the entire geographic extent of the TOM. Different studies show that the January 2005 and December 2006 SPEs had a strong effect on the TOM. The Seppälä et al. (2006, Figure 4) shows the TOM, observed at about 70-km altitude with maximum values of ~2 ppmv, which reduce to ~0.4 to 0.6 ppmv (80 to 70%) by 17–18 January 2005. This result was confirmed by the SIC model which predicted >70% O_3 loss between 70 and 80 km during the January 2005 SPE. Whereas Sofieva et al. (2009) report a drop in O_3 mixing ratios at 65–70 km from ~2 ppmv before the SPE to <0.5 ppmv after storm onset (>75%) for the December 2006 SPE. These results show a stronger depletion than our results, which show correlations of −0.56 and −0.60 ($r^2 = 31\%$ and 36%) for January 2005 and December 2006 SPEs, respectively, at SZAs 95°–105° (twilight conditions). At larger SZAs (115°–125°), however, our results for the January 2005 SPE show a higher correlation of −0.72 (52%).

The lack of correlation between EEP and O_3 mixing ratio reduction might be due to the viewing conditions of the MLS. The superposed epoch analyses shows, however, a lagged O_3 mixing ratio reduction in response to EEP and OH enhancement. A lagged response was also shown in the study by Turunen et al. (2016). Further, the distribution of the TOM is influenced by planetary waves, leading to longitudinal variations (Smith et al., 2018) more prominent in the NH winter. This makes it hard to see the direct impact of EEP on the tertiary O_3. The observed O_3 is that which might not have been reduced yet or might have already partly recovered.

The planetary waves/dynamics tend to transport the O_3 away from the auroral zone, leading to mixing. Nevertheless, the superposed epoch analysis including both OH and O_3 implies that there is evidence for a subtle impact of EEP on the TOM.

Therefore, for EEP to have an impact on O_3, it depends on a complex combination of the geographic intersection of the region of particle precipitation with the TOM, the distribution of the background atmospheric constituents, planetary waves, and time of precipitation. The combination of all these factors results in a much smaller impact on O_3 from EEP than from SPEs. To quantitatively assess how much of the energy deposition actually affects O_3 requires a combination of particle observations from different satellites, observing at different local times together with O_3 observations from different satellites at local times covering twilight conditions.

5. Summary and Conclusions

MLS is the only satellite-borne instrument that simultaneously measures OH and O_3, and hence allows to study if the apparent O_3 changes are correlated with OH. There are very few studies that observe EEP, OH, and O_3 simultaneously and therefore are able to verify that the changes observed in O_3 are due to OH enhancement produced by EEP and is not a change related to, for example, dynamics.

In this study we investigate when maximum overlap between the auroral zone and observation of the TOM exists. We further investigate when in time and where in location EEP is important for the variability in the TOM. By sorting the MLS data into five SZA bands, we use correlation analysis to find out the relationship between the variables OH, AE, energy deposition (protons and electrons), H_2O, and temperature in the different SZA bands of Aura MLS.

Our results show that maximum overlap between the auroral zone and the TOM exists during winter: January and December in the NH. In the periods considered, the months January 2005 and December 2006 are active with both SPEs and EEP events. Generally, there is limited overlap between the auroral zone where

EEP is expected and the location of the TOM which varies in size in the different winter months. Furthermore, there is limited overlap between the oval and the TOM when Aura MLS is observing in the SZA band of 95°–105° at which morning twilight conditions are expected.

Therefore, for SZA > 95° in the NH the Aura MLS barely observes the direct EEP-OH effect on the TOM. Within the auroral zone, the MLS instrument predominantly observes the O_3 that was impacted at evening twilight and it is yet to recover from the impact. This makes it tricky to make confident deductions on the EEP-OH impact on the TOM.

The case studies considered show that only a portion of the incident electron energy deposition will result in OH formation, as it appears to be strongly dependent on the geographic distribution of H_2O. Further, only a portion of the EEP-OH formed will be able to impact the TOM at twilight conditions depending on its geographic extent. This results in a much smaller EEP impact region within the geographic extent of the TOM as compared with the impact region of SPEs which cover almost the entire extent of the TOM. The correlation analysis also shows no significant relationship between electron precipitation and the TOM. The superposed epoch analysis, however, indicates O_3 mixing ratio decrease over the auroral zone lagged by 1 day compared to the maximum EEP-OH impact. This implies that the importance of EEP upon the O_3 mixing ratio is strongly influenced by the atmospheric background both in terms of chemistry and dynamics.

A quantitative assessment needs multisatellite measurements of both O_3 and EEP at different solar local times, covering evening to morning twilight conditions, to separate the direct EEP-OH effect on O_3 from the lagged effect. In the same respect, to quantify how much of the electron precipitation eventually affects O_3, observations at twilight conditions are required. It is also necessary to account for the variability due to the background atmospheric dynamics as they affect the O_3 distribution through H_2O and temperature, and redistribute the O_3 anomalies.

Acknowledgments
This study was supported by the Research Council of Norway under contract 223252/F50. The authors thank the NOAA's National Geophysical Data Center (NGDS) for providing NOAA data (https://satdat.ngdc.noaa.gov/), WDC Geomagnetism, Kyoto, Japan, for AE index (http://wdc.kugi.kyoto-u.ac.jp/wdc/Sec3.html), and NASA Goddard Earth Science Data and Information Services Center (GES DISC) for providing Aura/MLS data (https://mls.jpl.nasa.gov/).

References

Aikin, A. C., & Smith, H. J. P. (1999). Mesospheric constituent variations during electron precipitation events. *Journal of Geophysical Research*, *104*(D21), 26,457–26,471. https://doi.org/10.1029/1999JD900752

Andersson, M. E., Verronen, P. T., Rodger, C. J., Clilverd, M. A., & Seppälä, A. (2014a). Missing driver in the Sun-Earth connection from energetic electron precipitation impacts mesospheric ozone. *Nature Communications*, *5*(1), 5197. https://doi.org/10.1038/ncomms6197

Andersson, M. E., Verronen, P. T., Rodger, C. J., Clilverd, M. A., & Wang, S. (2014b). Longitudinal hotspots in the mesospheric OH variations due to energetic electron precipitation. *Atmospheric Chemistry and Physics*, *14*(2), 1095–1105. https://doi.org/10.5194/acp-14-1095-2014

Andersson, M. E., Verronen, P. T., Wang, S., Rodger, C. J., Clilverd, M. A., & Carson, B. R. (2012). Precipitating radiation belt electrons and enhancements of mesospheric hydroxyl during 2004–2009. *Journal of Geophysical Research*, *117*, D09304. https://doi.org/10.1029/2011JD017246

Bethe, H. A., & Ashkin, J. (1953). *Part II of experimental nuclear physics Edited by* E. Segre, Passage of radiations through matter (Vol. 1). New York: John Wiley & Sons.

Crutzen, P. J., & Solomon, S. (1980). Response of mesopheric ozone to particle precipitation. *Planetary and Space Science*, *28*(12), 1147–1153. https://doi.org/10.1016/0032-0633(80)90073-2

Damiani, A., Storini, M., Laurenza, M., & Rafanelli, C. (2008). Solar particle effects on minor components of the Polar atmosphere. *Annales Geophysicae*, *26*(2), 361–370. https://doi.org/10.5194/angeo-26-361-2008

Damiani, A., Storini, M., Santee, M. L., & Wang, S. (2010). Variability of the nighttime OH layer and mesospheric ozone at high latitudes during northern winter: Influence of meteorology. *Atmospheric Chemistry and Physics*, *10*(21), 10,291–10,303. https://doi.org/10.5194/acp-10-10291-2010

Evans, D., & Greer, M. (2000). *Polar orbiting environmental satellite space environment monitor - 2: Instrument descriptions and archive data documentation* (1.4 ed.). Boulder, Colorado: NOAA.

Fritsch, F. N., & Carlson, R. E. (1980). Monotone piecewise cubic interpolation, *17*(2), 238–246.

Hedin, A. E. (1991). Extension of the MSIS thermosphere model into the middle and lower atmosphere. *Journal of Geophysical Research*, *96*(A2), 1159–1172. https://doi.org/10.1029/90JA02125

Jackman, C. H., Marsh, D. R., Vitt, F. M., Roble, R. G., Randall, C. E., Bernath, P. F., et al. (2011). Northern Hemisphere atmospheric influence of the solar proton events and ground level enhancement in January 2005. *Atmospheric Chemistry and Physics*, *11*(13), 6153–6166. https://doi.org/10.5194/acp-11-6153-2011

Livesey, N. J., Read, W. G., Wagner, P. A., Froidevaux, L., Lambert, A., Manney, G. L., Millan Valle, L. F., Pumphrey, H. C., Santee, M. L., Schwartz, M. J., Wang, S., Fuller, R. A., Jarnot, R. F., Knosp, B. W., & Martinez, E.(2015). *Earth observing system(EOS) aura microwave limb sounder(MLS) version 4.2x level 2 data quality and description document*. Pasadena, California: California Institute of Technology. 91109-8099.

Marsh, D., Smith, A., Brasseur, G., Kaufmann, M., & Grossmann, K. (2001). The existence of a tertiary ozone maximum in the high-latitude middle mesosphere. *Geophysical Research Letters*, *28*(24), 4531–4534. https://doi.org/10.1029/2001GL013791

Nesse Tyssøy, H., Sandanger, M. I., Ødegaard, L. K. G., Stadsnes, J., Aasnes, A., & Zawedde, A. E. (2016). Energetic electron precipitation into the middle atmosphere—Constructing the loss cone fluxes from MEPED POES. *Journal of Geophysical Research: Space Physics*, *121*, 5693–5707. https://doi.org/10.1002/2016JA022752

Nesse Tyssøy, H., & Stadsnes, J. (2015). Cutoff latitude variation during solar proton events: Causes and consequences. *Journal of Geophysical Research: Space Physics*, *120*, 553–563. https://doi.org/10.1002/2014JA020508

Nesse Tyssøy, H., Stadsnes, J., Søraas, F., & Sørbø, M. (2013). Variations in cutoff latitude during the January 2012 solar proton event and implication for the distribution of particle energy deposition. *Geophysical Research Letters*, *40*, 4149–4153. https://doi.org/10.1002/grl.50815

Ødegaard, L. K. G., Tyssøy, H. N., Sandanger, M. I. J., Stadsnes, J., & Søraas, F. (2016). Space Weather impact on the degradation of NOAA POES MEPED proton detectors. *Journal of Space Weather and Space Climate*, *6*, A26. https://doi.org/10.1051/swsc/2016020

Ødegaard, L. K. G., Tyssøy, H. N., Søraas, F., Stadsnes, J., & Sandanger, M. I. (2017). Energetic electron precipitation in weak to moderate corotating interaction region-driven storms. *Journal of Geophysical Research: Space Physics*, *122*, 2900–2921. https://doi.org/10.1002/2016JA023096

Pickett, H. M., Read, W. G., Lee, K. K., & Yung, Y. L. (2006). Observation of night OH in the mesosphere. *Geophysical Research Letters*, *33*, L19808. https://doi.org/10.1029/2006GL026910

Rees, M. H. (1989). *Physics and chemistry of the upper atmosphere (Cambridge Atmospheric and Space Science Series)*. Cambridge: Cambridge University Press.

Rodger, C. J., Clilverd, M. A., Green, J. C., & Lam, M. M. (2010). Use of POES SEM-2 observations to examine radiation belt dynamics and energetic electron precipitation into the atmosphere. *Journal of Geophysical Research*, *115*, A04202. https://doi.org/10.1029/2008JA014023

Rodger, C. J., Kavanagh, A. J., Clilverd, M. A., & Marple, S. R. (2013). Comparison between POES energetic electron precipitation observations and riometer absorptions: Implications for determining true precipitation fluxes. *Journal of Geophysical Research: Space Physics*, *118*, 7810–7821. https://doi.org/10.1002/2013JA019439

Rusch, D., Grard, J. C., Solomon, S., Crutzen, P., & Reid, G. (1981). The effect of particle precipitation events on the neutral and ion chemistry of the middle atmosphere—I. Odd nitrogen. *Planetary and Space Science*, *2*(7), 767–774. https://doi.org/10.1016/0032-0633(81)90048-9

Sandanger, M. I., Ødegaard, L. K. G., Tyssøy, H. N., Stadsnes, J., Søraas, F., Oksavik, K., & Aarsnes, K. (2015). In flight calibration of NOAA POES proton detectors—Derivation of the MEPED correction factors. *Journal of Geophysical Research: Space Physics*, *120*, 9578–9593. https://doi.org/10.1002/2015JA021388

Schoeberl, M., Douglass, A., Hilsenrath, E., Bhartia, P., Beer, R., Waters, J., et al. (2006). Overview of the EOS Aura mission. *Geoscience and Remote Sensing, IEEE Transactions On*, *44*(5), 1066–1074. https://doi.org/10.1109/TGRS.2005.861950

Seppälä, A., Verronen, P. T., Sofieva, V. F., Tamminen, J., Kyrölä, E., Rodger, C. J., & Clilverd, M. A. (2006). Destruction of the tertiary ozone maximum during a solar proton event. *Geophysical Research Letters*, *33*, L07804. https://doi.org/10.1029/2005GL025571

Smith, A. K., Espy, P. J., López-Puertas, M., & Tweedy, O. V. (2018). Spatial and temporal structure of the tertiary ozone maximum in the polar winter mesosphere. *Journal of Geophysical Research: Atmospheres*, *123*, 4373–4389. https://doi.org/10.1029/2017JD028030

Smith, A. K., López-Puertas, M., García-Comas, M., & Tukiainen, S. (2009). SABER observations of mesospheric ozone during NH late winter 2002–2009. *Geophysical Research Letters*, *36*, L23804. https://doi.org/10.1029/2009GL040942

Sofieva, V. F., Kalakoski, N., Verronen, P. T., Päivärinta, S. M., Kyrölä, E., Backman, L., & Tamminen, J. (2012). Polar-night O_3, NO_2 and NO_3 distributions during sudden stratospheric warmings in 2003–2008 as seen by GOMOS/Envisat. *Atmospheric Chemistry and Physics*, *12*(2), 1051–1066. https://doi.org/10.5194/acp-12-1051-2012

Sofieva, V. F., Kyrölä, E., Verronen, P. T., Seppälä, A., Tamminen, J., Marsh, D. R., et al. (2009). Spatio-temporal observations of the tertiary ozone maximum. *Atmospheric Chemistry and Physics*, *9*(13), 4439–4445. https://doi.org/10.5194/acp-9-4439-2009

Solomon, S., Reid, G. C., Rusch, D. W., & Thomas, R. J. (1983). Mesospheric ozone depletion during the solar proton event of July 13, 1982 Part II. Comparison between theory and measurements. *Geophysical Research Letters*, *10*(4), 257–260. https://doi.org/10.1029/GL010i004p00257

Solomon, S., Rusch, D., Gérard, J., Reid, G., & Crutzen, P. (1981). The effect of particle precipitation events on the neutral and ion chemistry of the middle atmosphere: II. Odd hydrogen. *Planetary and Space Science*, *29*(8), 885–893. https://doi.org/10.1016/0032-0633(81)90078-7

Sonnemann, G., Grygalashvyly, M., Hartogh, P., & Jarchow, C. (2006). Behavior of mesospheric ozone under nearly polar night conditions. *Advances in Space Research*, *38*(11), 2402–2407. https://doi.org/10.1016/j.asr.2006.09.011

Thorne, R. (1980). The importance of energetic particle precipitation on the chemical composition of the middle atmosphere. *Pure and Applied Geophysics*, *118*(1), 128–151. https://doi.org/10.1007/BF01586448

Turunen, E., Kero, A., Verronen, P. T., Miyoshi, Y., Oyama, S. I., & Saito, S. (2016). Mesospheric ozone destruction by high-energy electron precipitation associated with pulsating aurora. *Journal of Geophysical Research: Atmospheres*, *121*, 11,852–11,861. https://doi.org/10.1002/2016JD025015

Verkhoglyadova, O. P., Wang, S., Mlynczak, M. G., Hunt, L. A., & Zank, G. P. (2015). Effects of two large solar energetic particle events on middle atmosphere nighttime odd hydrogen and ozone content: Aura/MLS and TIMED/SABER measurements. *Journal of Geophysical Research: Space Physics*, *120*, 12–29. https://doi.org/10.1002/2014JA020609

Verkhoglyadova, O. P., Wissing, J. M., Wang, S., Kallenrode, M. B., & Zank, G. P. (2016). Nighttime mesospheric hydroxyl enhancements during SEP events and accompanying geomagnetic storms: Ionization rate modeling and Aura satellite observations. *Journal of Geophysical Research: Space Physics*, *121*, 6017–6030. https://doi.org/10.1002/2015JA022217

Verronen, P. T., Andersson, M., Rodger, C., Clilverd, M., Wang, S., & Turunen, E. (2013). Comparison of modeled and observed effects of radiation belt electron precipitation on mesospheric hydroxyl and ozone. *Journal of Geophysical Research: Atmospheres*, *118*, 11,419–11,428. https://doi.org/10.1002/jgrd.50845

Verronen, P. T., Rodger, C. J., Clilverd, M. A., & Wang, S. (2011). First evidence of mesospheric hydroxyl response to electron precipitation from the radiation belts. *Journal of Geophysical Research*, *116*, D07307. https://doi.org/10.1029/2010JD014965

Verronen, P. T., Seppälä, A., Kyrölä, E., Tamminen, J., Pickett, H. M., & Turunen, E. (2006). Production of odd hydrogen in the mesosphere during the January 2005 solar proton event. *Geophysical Research Letters*, *33*, L24811. https://doi.org/10.1029/2006GL028115

Waters, J. W., Froidevaux, L., Harwood, R. S., Jarnot, R. F., Pickett, H. M., Read, W. G., et al. (2006). The Earth observing system microwave limb sounder (EOS MLS) on the Aura Satellite. *IEEE Transactions on Geoscience and Remote Sensing*, *44*(5), 1075–1092. https://doi.org/10.1109/TGRS.2006.873771

Zawedde, A. E., Nesse Tyssøy, H., Hibbins, R., Espy, P. J., Ødegaard, L. K. G., Sandanger, M. I., & Stadsnes, J. (2016). The impact of energetic electron precipitation on mesospheric hydroxyl during a year of solar minimum. *Journal of Geophysical Research: Space Physics*, *121*, 5914–5929. https://doi.org/10.1002/2016JA022371

Zawedde, A. E., Nesse Tyssøy, H., Stadsnes, J., & Sandanger, M. I. (2018). The impact of energetic particle precipitation on mesospheric OH—Variability of the sources and the background atmosphere. *Journal of Geophysical Research: Space Physics*, *123*, 5764–5789. https://doi.org/10.1029/2017JA025038